CrossMark

ORIGINAL ARTICLE

Central connectivity of the chorda tympani afferent terminals in the rat rostral nucleus of the solitary tract

Sook Kyung Park · Dae Seop Lee · Jin Young Bae · Yong Chul Bae

Abstract The rostral nucleus of the solitary tract (rNST) receives gustatory input via chorda tympani (CT) afferents from the anterior two-thirds of the tongue and transmits it to higher brain regions. To help understand how the gustatory information is processed at the 1st relay nucleus of the brain stem, we investigated the central connectivity of the CT afferent terminals in the central subdivision of the rat rNST through retrograde labeling with horseradish peroxidase, immunogold staining for GABA, glycine, and glutamate, and quantitative ultrastructural analysis. Most CT afferents were small myelinated fibers (<5 μm^2 in cross-sectional area) and made simple synaptic arrangements with 1–2 postsynaptic dendrites. It suggests that the gustatory signal is relayed to a specific group of neurons with a small degree of synaptic divergence. The volume of the identified synaptic boutons was positively correlated with their mitochondrial volume and active zone area, and also with the number of their postsynaptic dendrites. One-fourth of the boutons received synapses from GABA-immunopositive presynaptic profiles, 27 % of which were also glycine-immunopositive. These results suggest that the gustatory information mediated by CT afferents to the rNST is processed in a simple and specific manner. They also suggest that the minority of CT afferents are presynaptically modulated by GABA- and/or glycine-mediated mechanism.

Abbreviations

CT	Chorda tympani
EM	Electron microscopy
GG	Geniculate ganglion
Glut	Glutamate
Gly	Glycine
HRP	Horseradish peroxidase
HTM	High threshold mechanoreceptive
LDCV	Large dense core vesicle
LM	Light microscopy
LTM	Low threshold mechanoreceptive
PATs	Primary afferent terminals
rNST	Rostral nucleus of the solitary tract
SDH	Spinal dorsal horn
TSN	Trigeminal sensory nuclei

S. K. Park and D. S. Lee contributed equally to this work.

S. K. Park · D. S. Lee · J. Y. Bae · Y. C. Bae (✉)
Department of Anatomy and Neurobiology, School of Dentistry, Kyungpook National University, 188-1, 2-Ga, Samdeok-Dong, Jung-Gu, Daegu 700-412, Korea
e-mail: ycbae@knu.ac.kr

Introduction

The central connectivity of sensory primary afferent terminals (PATs) varies according to the type of the primary afferents they originate. Thus, terminals of Aδ high threshold mechanoreceptive (HTM) afferents, which have diverse response properties, contact 3–13 postsynaptic dendrites and thus form a divergent afferent system (Alvarez et al. 1992), whereas terminals of proprioceptive afferents, which mostly underlie simple motor reflexes, contact one or two postsynaptic dendrites (Bae et al. 1996; Kishimoto et al. 1998; Zhang et al. 2003). On the other hand, terminals of Aδ HTM and Aβ low threshold

🖄 Springer

mechanoreceptive (LTM) afferents, which carry sensory input with high spatial discriminative properties, frequently receive axoaxonic synapses (Alvarez et al. 1992; Watson et al. 2002; Bae et al. 2005a), whereas terminals of peptidergic C afferents, which carry sensory input with poor spatial resolution, do not (Alvarez et al. 1993). In these axoaxonic synapses, the axon terminals that are presynaptic to PATs are small and contain GABA and/or glycine, suggesting fine inhibitory presynaptic modulation of PATs (Watson 2004; Bae et al. 2005b; Moon et al. 2008). The central connectivity of sensory primary afferents within the same class also varies according to their target nuclei (Fyffe and Light 1984; Walmsley et al. 1987, 1995; Bae et al. 1994, 2005a). For example, terminals of LTM afferents have more complex synaptic connectivity and receive more extensive presynaptic modulation in the principal trigeminal nucleus, which is involved in the discriminative aspect of the sensory information, than in the oral nucleus, which is involved in the reflexive motor function (Bae et al. 1994; Zhang et al. 2001).

The chorda tympani (CT) afferent conveys sensory information, mainly taste and partly temperature and touch, from the anterior tongue to the rostral nucleus of the solitary tract (rNST, Ogawa et al. 1968; Biedenbach and Chan 1971; Matsuo et al. 1995). CT afferent terminals in the rNST frequently form synapses onto small size postsynaptic dendrites and receive synapses from vesicle-containing profiles, suggesting that the gustatory information conveyed via the CT is presynaptically modulated before being transmitted to the distal part of the dendritic tree of the postsynaptic neurons (Whitehead 1986; May et al. 2007; Wang et al. 2012).

The gustatory sense, conveyed via Aδ fibers (Iriuchijima and Zotterman 1961), differs from the somatic sense conveyed via the same type of fibers in their conduction velocity, sensory properties, and associated neural circuits (Lawson and Waddell 1991; Matsuo et al. 1995; for review, see Craig 2002; Almeida et al. 2004), suggesting that it is processed in a distinctive manner. The ultrastructural features of the CT afferent terminals in the rNST have been studied previously (Whitehead 1986, 1993; Davis 1998; May et al. 2007; Wang et al. 2012). Also, studies of the morphology and distribution of GABAergic neurons in the rNST (Lasiter and Kachele 1988; Davis 1993; Wetherton et al. 1998; Leonard et al. 1999) have revealed that the inhibitory and the excitatory responses of taste-sensitive neurons are mediated by GABA and glutamate, respectively (Wang and Bradley 1995; for review, see Smith et al. 1998). Further information on the synaptic connectivity of the CT afferent terminals in the rNST, their ultrastructural features related to synaptic release, and their neurochemistry, may help understand how the gustatory

information is processed at the 1st relay nucleus of the brain stem.

In this study, we investigated the central connectivity of the CT afferent terminals and their associated neurochemicals in the central subdivision of the rat rNST through retrograde labeling with horseradish peroxidase, immunogold staining for GABA, glycine, and glutamate, and quantitative ultrastructural analysis.

Materials and methods

Labeling of chorda tympani afferents and tissue preparation

All animal procedures were performed according to the National Institute of Health guidelines and were approved by the Kyungpook National University Intramural Animal Care and Use Committee. Three male Sprague–Dawley rats weighing 300–350 g were used for this study. Animals were anesthetized with sodium pentobarbital (40 mg/kg, I.P.) and placed on a water-circulating pad to maintain body temperature at 36 °C. Animals were stabilized in a non-traumatic head holder, and a small hole was made in the tympani bulla to expose the CT nerve. The CT was sectioned distally to the geniculate ganglion (GG) and crystals of horseradish peroxidase (HRP, TOYOBO Co., Japan) were applied to the central stump of the nerve, and sealed with silicone-casting compound (Kwik-Cast, World Precision Instruments) to prevent spreading of HRP in the surrounding tissues, and then the skin incision was sutured and the animals allowed to recover.

After 24 h, the rats were deeply reanesthetized with sodium pentobarbital (80 mg/kg, I.P.) and perfused transcardially with freshly prepared fixative containing 2.5 % glutaraldehyde, 1 % paraformaldehyde, and 0.1 % picric acid in 0.1 M phosphate buffer (PB, pH 7.4). The brain stem, GG and its proximal sensory root were removed, postfixed in the same fixative for 2 h at 4 °C, and cut on a Vibratome at 60 μm. HRP was visualized according to tungstate/tetramethylbenzidine protocol (Weinberg and van Eyck 1991) and stabilized with diaminobenzidine in 0.1 M PB (pH 6.0).

For light microscopy (LM), sections containing HRP-labeled somata in the GG were lightly counterstained with cresyl fast violet. For electron microscopy (EM), sections containing HRP-labeled puncta in the rNST and proximal sensory root of the GG were postfixed with 0.5 % osmium tetroxide in PB for 30 min, dehydrated in the graded alcohols, flat embedded in Durcupan ACM (Fluka, Buchs, Switzerland) between strips of Aclar plastic film (EMS), and cured for 48 h at 60 °C. For analysis of the HRP-

labeled terminals in the rNST, chips of the areas containing dense HRP labeling in the central subdivision of the rNST in two 60 μm thick Vibratome sections per animal were cut and glued onto blank resin block with cyanoacrylate. One hundred to one hundred and fifty serial ultrathin sections per block were collected on formvar-coated single slot nickel grids and stained with uranyl acetate and lead citrate. Series of grids containing serial sections were examined on a Hitachi H-7500 electron microscope (Hitachi, Tokyo, Japan). We defined the central subdivision of rNST according to the description by Corson et al. (2012). It contained more thin myelinated fibers and denser small cells than the lateral and ventral subdivisions of the nucleus.

Morphometric analysis of the geniculate ganglion neurons and chorda tympani afferents

For LM analysis of somata of GG neurons, light micrographs were obtained with an Exi digital camera (Q-Imaging Inc., Surrey, CA, USA) attached to a Zeiss Axioplan 2 microscope (Carl Zeiss, Gottingen, Germany) and saved as TIFF files. The cross-sectional areas of a total of 267 HRP-labeled neurons and 484 unlabeled neurons with clearly visible nucleoli from three GG were measured using Image J software (v 1.45; NIH, Bethesda, MD, USA), and graphs were built in Kaleidagraph (v 3.5; Synergy Software, Reading, PA, USA). Inter-animal variability in cross-sectional area was not significant (one-way ANOVA), and the data could be pooled for analysis.

For EM analysis of CT afferents and their terminals, images were taken from random sections containing HRP-labeled axons in the proximal sensory root of the GG and from every other section in serial sections of each HRP-labeled bouton in the central subdivision of the rNST with a DigitalMicrograph software driving a cooled CCD camera (SC1000; Gatan, Pleasanton, CA, USA) attached to the microscope, and saved as TIFF files. For analysis of labeled boutons, after labeled boutons were identified on one of the serial sections, they were followed up through the entire series of sections containing those boutons.

The cross-sectional area of HRP-labeled axons in the proximal sensory root of GG was measured in electron micrographs at $10,000\times$ or $15,000\times$ original magnifications. Immunopositive fibers were grouped into unmyelinated, small myelinated (<20 μm^2 cross-sectional area, equivalent to <5 μm in diameter) and large myelinated fibers (>20 μm^2 cross-sectional area, equivalent to >5 μm in diameter), corresponding to C, Aδ, and Aα/β fibers, respectively (Barret et al. 2009; Debanne et al. 2011). Bouton volume and active zone areas of HRP-labeled boutons were calculated by measuring each cross-sectional area and the length of the active zone, respectively,

assuming an average section thickness of 75 nm. Vesicle density was calculated by counting the number of vesicles per cross-sectional area of the bouton in one section through the series, which contained the largest number of vesicles. Measurements were performed on electron micrographs at $30,000\times$ original magnification using the Image J software. Correlation analysis with Fisher's r to z transformation for significance and unpaired Student's t test was used to test relationships. Inter-animal variability in frequency of occurrence of different types of contacts per HRP-labeled chorda tympani afferent bouton, and proportion of each type of HRP-labeled axon was insignificant (one-way ANOVA), and the data could be pooled for analysis.

Postembedding immunogold staining and quantitative analysis

Sections were immunostained for GABA, glycine (Gly), and glutamate (Glut) by the postembedding immunogold method, as previously published from our laboratory (Bae et al. 2002; Paik et al. 2007). Briefly, the grids were treated for 10 min in 1 % periodic acid, to etch the resin, and for 15 min in 9 % sodium periodate, to remove the osmium tetroxide. Then the grids were washed in distilled water, transferred to tris-buffered saline containing 0.1 % triton X-100 (TBST; pH 7.4) for 10 min, and incubated in 2 % human serum albumin (HSA) in TBST for 10 min. The grids were then incubated with rabbit antisera against GABA (GABA 990, 1:800), glycine (Gly 290, 1:280), or glutamate (Glut 607, 1:1,100) in TBST containing 2 % HSA for 2 h at room temperature. To eliminate cross-reactivity, the diluted antisera were pre-adsorbed overnight with glutaraldehyde (G)-conjugated amino acids (500 μM Glut-G for GABA, 300 μM β-alanine-G and 200 μM GABA-G for Gly, 300 μM glutamine-G, 100 μM aspartate-G, and 200 μM β-alanine-G for Glut; Ottersen et al. 1986). After extensive rinsing in TBST, grids were incubated for 3 h in goat anti-rabbit IgG coupled to 15 nm gold particles (1:25 in TBST containing 0.05 % polyethylene glycol; BioCell Co., Cardiff, UK). After a rinse in distilled water, the grids were counterstained with uranyl acetate and lead citrate and examined on a Hitachi H-7500 electron microscope (Hitachi, Tokyo, Japan) at 80 kV accelerating voltage. Images were saved as TIFF files, and brightness and contrast were adjusted in Photoshop CS3 (Adobe Systems, San Jose, CA, USA).

To quantify the immunoreactivity for GABA and Gly, gold particle density (number of gold particles per μm^2) of p-endings of presumed axonal origin or that of vesicle-rich areas of p-profiles of presumed dendritic origin was compared with "background" density. Background was defined as particle density of boutons containing clear round

vesicles and establishing synapses of asymmetric type with dendrites or somata in the same sections. Presynaptic p-endings or p-profiles were considered GABA- and/or Gly-immunopositive if the gold particle density for the respective antigen was at least five times higher than "background" density. To assess the immunoreactivity for Glut, we compared gold particle density over HRP-labeled boutons to the average tissue density in 10–20 randomly selected areas of 2 μm^2 each (a total area of 20–40 μm^2) per section. Boutons containing gold particles at a density >2.576 SD of the average tissue density (99 % confidence level) were considered Glut-immunopositive (Shigenaga et al. 2005; Paik et al. 2012). Immunogold labeling over mitochondrial profiles was excluded from all measurements.

Antibodies characterization

The antisera used in this study were raised according to the procedure of Storm-Mathisen et al. (1983), with the modification that GABA, Gly, and Glut were conjugated to bovine serum albumin (BSA) by glutaraldehyde and formaldehyde (instead of glutaraldehyde alone). These antisera (a kind gift from professor O.P. Ottersen at the Center for Molecular Biology and Neuroscience, University of Oslo) have been extensively characterized (Ottersen 1989a; Takumi et al. 1999) and routinely used in our previous works (Bae et al. 2000, 2002; Paik et al. 2007, 2011). Their specificity was also confirmed on thin sections of 'sandwiches' of rat brain macromolecule–glutaraldehyde fixation complexes of different amino acids, including GABA, glutamate, taurine, glycine, aspartate, glutamine, and none (Ottersen 1987; Bae et al. 2000). Test sections were incubated in the same drops of GABA, Gly, and Glut antisera as tissue sections and the respective conjugates in the test sections were selectively labeled. Omission or replacement of the primary antisera with normal rabbit serum or pre-adsorption of the diluted anti-GABA serum with 200 μM GABA-G, the anti-Gly serum with 300 μM Gly-G, and the anti-Glut serum with 300 μM Glut-G, abolished the immunolabeling. Selectivity of immunolabeling was also confirmed in adjacent serial thin sections of the same boutons.

Results

At LM, most HRP-labeled neuronal somata in the geniculate ganglion (GG) were small (<400 μm^2: 89.5 %, Fig. 1). At EM, HRP-labeled axons in the proximal sensory root of the GG were mostly small myelinated fibers (<20 μm^2 in cross sectional area, equivalent to <5 μm in diameter: 89.5 %) and most of those (91 %) were among

the thinnest myelinated fibers (<5 μm^2 in cross-sectional area, equivalent to <2.6 μm in diameter). Labeled unmyelinated fibers (10.2 %) and a few large myelinated fibers (>20 μm^2 in cross sectional area, equivalent to >5 μm in diameter: 0.3 %, Fig. 2) were also observed.

HRP-labeled axons and boutons were dense in rNST (Fig. 3). We analyzed 44 HRP-labeled boutons reconstructed from serial sections in the central subdivision of the rNST at its middle or rostral level: Most labeled boutons had an elongated or scalloped shape and contained clear round vesicles of uniform size (45–55 nm in diameter) and often large dense core vesicles (∼18 % of the labeled boutons contained ≥5 such vesicles). Labeled boutons formed synapses onto small- or medium-sized dendritic shafts or spines which usually do not contain mitochondria, microtubules or neurofilaments and sometimes exhibit fuzzy cytoplasm (Fig. 4). Labeled boutons did not form synapses on primary dendrites or somata. On average, labeled boutons made synaptic contacts with 1.95 postsynaptic dendritic shafts or spines and 0.25 vesicle-containing profiles (Table 1). Most labeled boutons made synaptic contact with 1–2 and some up to 4 dendrites (Table 2), and about 30 % synapsed on dendritic spines (Table 1). Also, 25 % of the labeled boutons received synaptic contacts of symmetrical type from presynaptic vesicle-containing profiles (p-profiles). Most p-profiles were small presynaptic endings (p-endings) of presumed axonal origin that contained densely packed pleomorphic vesicles and never received synaptic contacts from other axonal endings (Figs. 4C1–2, 5). Some p-profiles were of presumed dendritic origin that contained sparse vesicles clustered around the presynaptic site, and occasionally ribosomes or smooth endoplasmic reticulum (Fig. 5C1–3).

Further analysis of 30 labeled boutons and 10 p-endings of presumed axonal origin revealed that several ultrastructural features related to synaptic release, including the bouton volume, mitochondrial volume, and active zone area, but not vesicle density, were significantly larger for the labeled boutons than for the p-endings (Table 3). The volume of the labeled boutons was positively correlated with the mitochondrial volume, active zone area, and the number of postsynaptic dendrites (Fig. 6).

Immunostaining of 45 p-profiles revealed that they were all immunopositive for GABA, 27 % were also immunopositive for glycine, and none were immunopositive for glycine only (Table 4). The density of gold particles coding for GABA or glycine was 5.4–35.8 and 5.5–12.9 times higher in p-profiles than background, respectively (Figs. 5, 7). On the other hand, all labeled boutons examined were glutamate immunopositive. The density of gold particles coding for glutamate measured in 10 labeled boutons was 1.9–4.0 times higher in HRP-labeled boutons than average tissue density (Fig. 8).

Fig. 1 HRP-labeled neurons of chorda tympani afferents in the geniculate ganglion (**a**, *arrows*) and their size distribution (**b**). Most labeled somata were small (<400 μm^2). *Scale bar* 50 μm
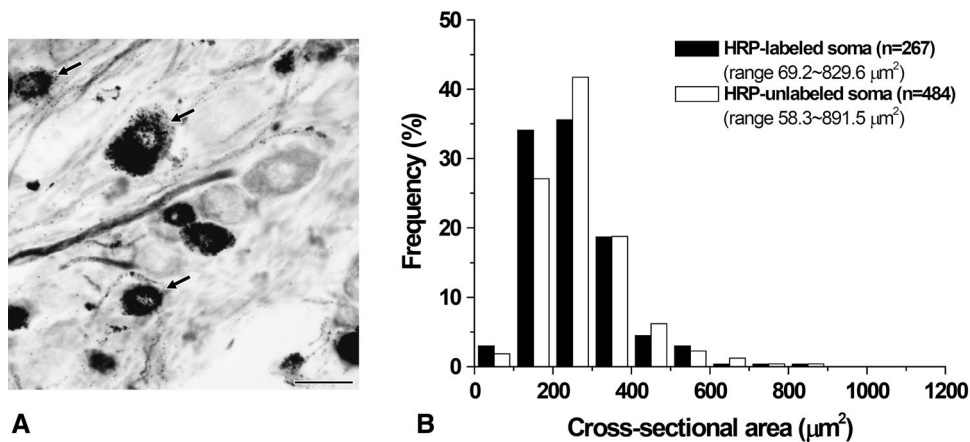

Fig. 2 HRP-labeled axons in the proximal root of the geniculate ganglion. **a–d** Electron micrographs showing HRP-labeled small myelinated, unmyelinated and large myelinated axons. **e**, **f** Histograms showing the proportion (**e**) and size distribution (**f**) of HRP-labeled myelinated and unmyelinated axons: Most (~90 %, **e**, **f**) of the labeled chorda tympani axons were small myelinated (<20 μm^2 in cross-sectional area, equivalent to 5 μm in diameter, left to the *dotted line* in **f**) and the rest were unmyelinated. *Arrows* HRP-labeled small myelinated axon (**a**, **b**). *Arrowhead* HRP-labeled unmyelinated axon (**c**). *Double arrows* HRP-labeled large myelinated axon (**d**). *Scale bar* 1 μm
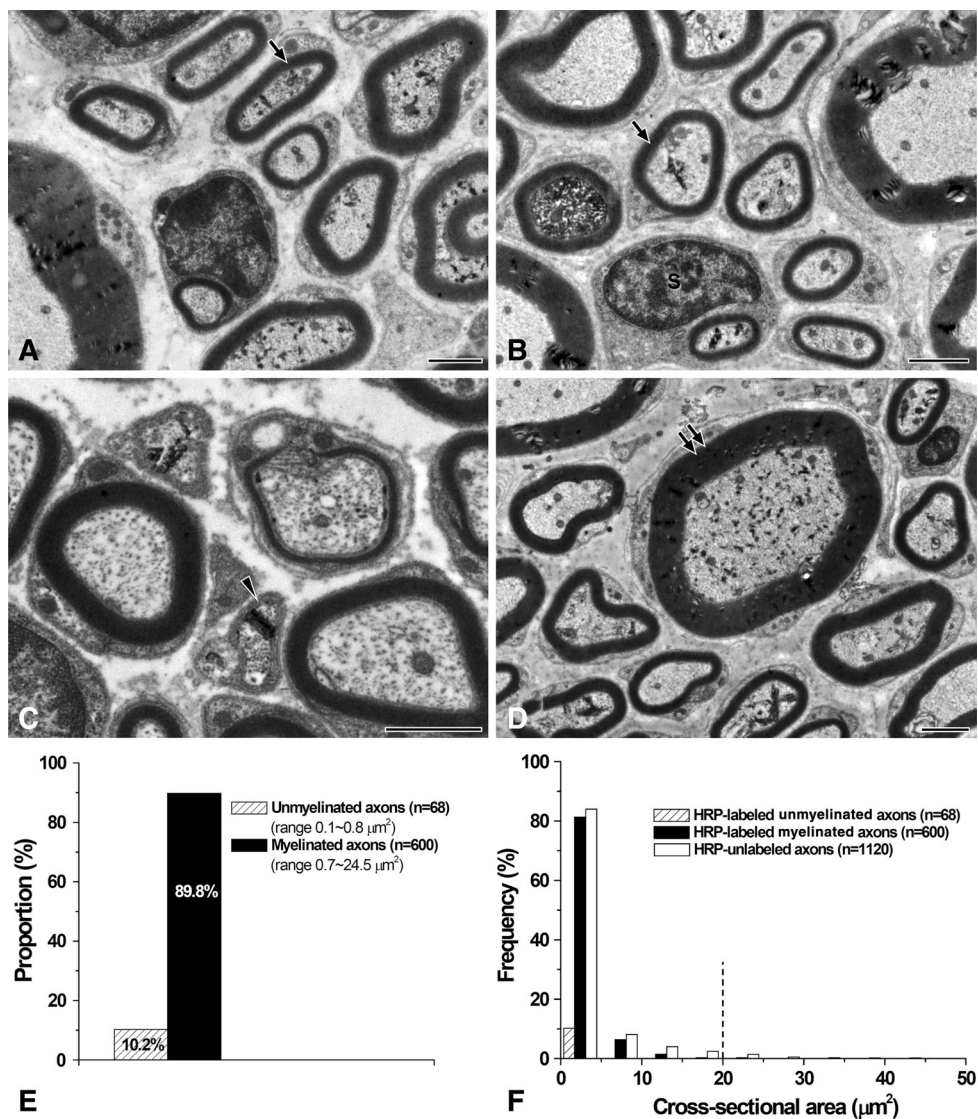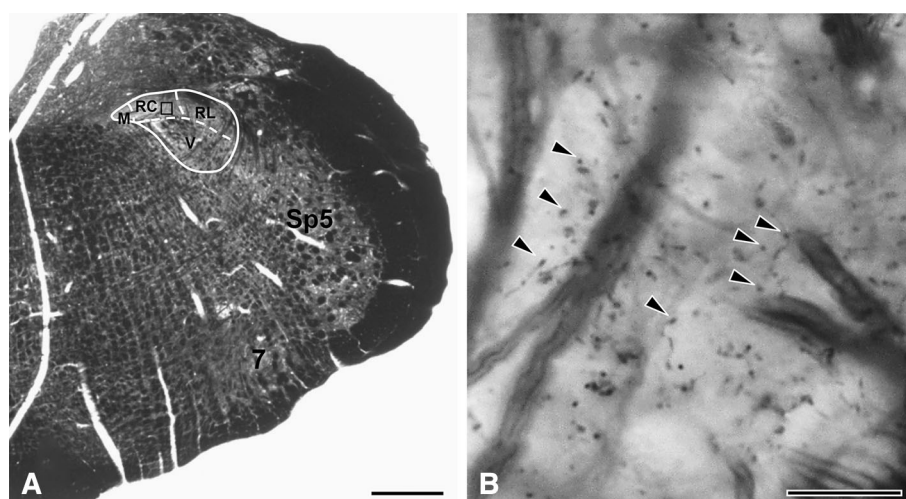
Fig. 3 Light micrographs showings HRP-labeled chorda tympani afferent boutons in the central subdivision of the rostral nucleus of the solitary tract (rNST). *Lines* in **a** demarcate the rough borders of the subdivisions in the rNST. **b** Enlargement of the *boxed area* in central subdivision of rNST in **a**. *Arrowheads* in **b** indicate HRP-labeled boutons. *M* medial subdivision of the rNST, *RC* central subdivision of the rNST, *RL* lateral subdivision of the rNST, *V* ventral subdivision of the rNST. *Sp5* spinal trigeminal nucleus, *7* facial nucleus. *Scale bars* 500 μm in **a**; 20 μm in **b**

Discussion

The main findings of the present study are as follows: (1) Most of the labeled axons were small myelinated Aδ fibers, which were associated with small-sized soma in the GG. (2) Most CT afferent boutons in the central subdivision of the rNST made synaptic contacts with one or two post-synaptic dendrites. (3) All p-profiles presynaptic to CT afferent boutons were GABA+ and considerable fractions were also glycine+. (4) The volume of the CT boutons was positively correlated with the mitochondrial volume, active zone area, and the number of postsynaptic dendrites.

The large majority of labeled neuronal somata in the GG had cross-sectional area of <400 μm^2. This is smaller than that of the somatosensory Aδ afferent neurons (400–1,100 μm^2) and within the size range of the C afferent neurons (<600 μm^2, Harper and Lawson 1985; Lawson et al. 1997, 2002). Also, most labeled myelinated fibers were smaller than 2.6 μm in diameter, within the range of the thinnest somatosensory myelinated Aδ fibers (2–5 μm in diameter, Grant 2006; Barret et al. 2009). This may corroborate the evidence that the taste-sensitive Aδ fibers have lower conduction velocity than the somatosensory Aδ fibers (Lawson and Waddell 1991; Matsuo et al. 1995). This also suggests that taste, conveyed via gustatory Aδ fibers, may be conducted more slowly than the sharp, localized pain, conveyed via the somatosensory Aδ fibers.

Most labeled boutons in the central subdivision of the rNST are presumed to arise from Aδ gustatory afferents. This assumption is based on (1) labeled axons in the CT

nerve which were almost exclusively small myelinated fibers, and almost all the taste responding fibers in the CT nerve were shown to be Aδ fibers (Iriuchijima and Zotterman 1961), whereas most of the unmyelinated fibers in the CT nerve have been shown to be parasympathetic secretomotor fibers (Farbman and Hellekant 1978); (2) the central subdivision of the rNST receiving mostly gustatory input via Aδ fibers, whereas the lateral subdivision receives mechanosensory input via Aβ fibers (Ogawa et al. 1984; Travers and Norgren 1995; King 2006); (3) the majority of the CT afferents are sensitive to taste and some CT afferents are thermosensitive or mechanosensitive only (Iriuchijima and Zotterman 1961; Biedenbach and Chan 1971; Matsuo et al. 1995). Moreover, many of the taste-sensitive fibers were also shown to respond to thermal and mechanical stimuli (Ogawa et al. 1968; Robinson 1988; Matsuo et al. 1995).

The ultrastructural features of the geniculate ganglion neurons and the CT afferent terminals in the rNST, involved in the processing of gustatory information, have been described previously: they contain round vesicles, usually make synapses onto middle-sized dendrites, and receive axoaxonic synapses from endings containing pleomorphic vesicles (Kitamura et al. 1982; Spassova 1983; Whitehead 1986, 1993; Davis 1998; May et al. 2007; Wang et al. 2012). We confirmed these observations and further elaborated on their unique central connectivity, based on reconstruction of serial sections. We interpret our findings to mean that taste information is processed in a unique manner in the 1st relay nucleus that differs from the processing of somatosensory information conveyed via

Fig. 4 Electron micrographs of serial thin sections showing HRP-labeled chorda tympani afferent boutons (*asterisks*) in the central subdivision of the rostral nucleus of the solitary tract. *Arrows* indicate HRP reaction product, *arrowheads* indicate synapses. **a1**, **a2** The labeled bouton contains clear round vesicles and makes an asymmetric synaptic contact with a dendritic shaft (*d*). **b1**, **b2** A labeled bouton establishes asymmetric synaptic contacts with a dendritic shaft (*d*) and a dendritic spine (*ds*). **c1**, **c2** A labeled bouton is presynaptic to a dendritic spine (*ds*) and also receives a synaptic contact from an axonal ending (*p*, the labeled bouton and the presynaptic axonal ending are outlined with a *dashed line*). *Scale bars* 500 nm
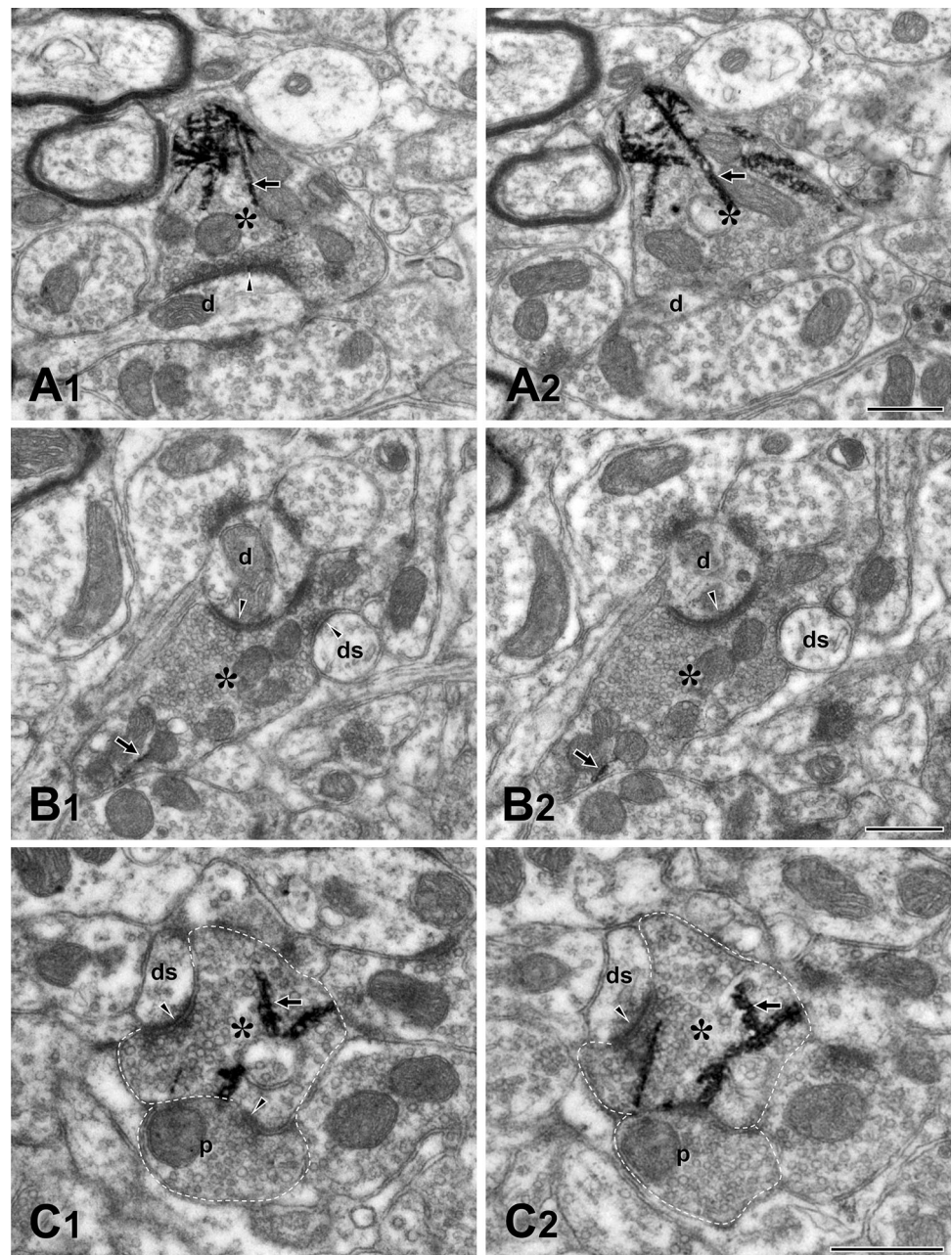

Table 1 Frequency of occurrence of different synaptic contacts of chorda tympani afferent boutons in the central subdivision of the rostral nucleus of the solitary tract (number of animals sampled, 3)

Number of labeled boutons	Synaptic contacts with					Total number of synaptic contacts
	Soma or primary dendrites	Dendritic			p-profiles	
		Shafts	Spines	Shafts or spines		
44	0.00 ± 0.00[a]	1.61 ± 0.99	0.34 ± 0.57	1.95 ± 0.96	0.25 ± 0.44	2.20 ± 1.15
n	0	71	15	86	11	97

*n* total number of synaptic contacts by all labeled boutons

[a] Values are Mean ± SD

Table 2 Frequency of postsynaptic dendrites and presynaptic profiles (p-profiles) of chorda tympani afferent boutons in the central subdivision of the rostral nucleus of the solitary tract (number of animals sampled, 3)

No. of labeled boutons	No. of postsynaptic dendrites					No. of p-profiles	
	1	2	3	4	5 or more	0	1
44	38.6 %	36.4 %	15.9 %	9.1 %	0.0 %	75.0 %	25.0 %
n	17/44	16/44	7/44	4/44	0/44	33/44	11/44

n number of boutons according to the number of their postsynaptic dendrites or presynaptic p-profiles/total number of examined boutons

Fig. 5 Electron micrographs of serial thin sections showing HRP-labeled chorda tympani afferent boutons (*asterisks*) in the central subdivision of the rostral nucleus of the solitary tract. Adjacent ultrathin sections of labeled boutons are immunostained for *GABA* (**a1**, **b1**, **c1**) and glycine (*Gly*, **a2**, **b2**, **c2**). **a1**, **a2** A labeled bouton forms synaptic contact with a small-sized dendrite (*d*) and also receives a synapse from a presynaptic p-ending (*p*), which shows immunoreactivity for GABA only. **b1**, **b2** A labeled bouton receives a synapse from a presynaptic p-ending (*p*) showing immunoreactivity for both GABA and glycine. **c1**–**c3** A labeled bouton receives a synapse from a presynaptic profile of dendritic origin (*d*) showing immunoreactivity for both GABA and glycine. The section from which C3 was taken was treated with EM stain only without immunogold staining. *Arrows* indicate HRP reaction product, *arrowheads* indicate synapses; the labeled bouton and/or the presynaptic p-ending are outlined with a *dashed line*. *Scale bar* 500 nm
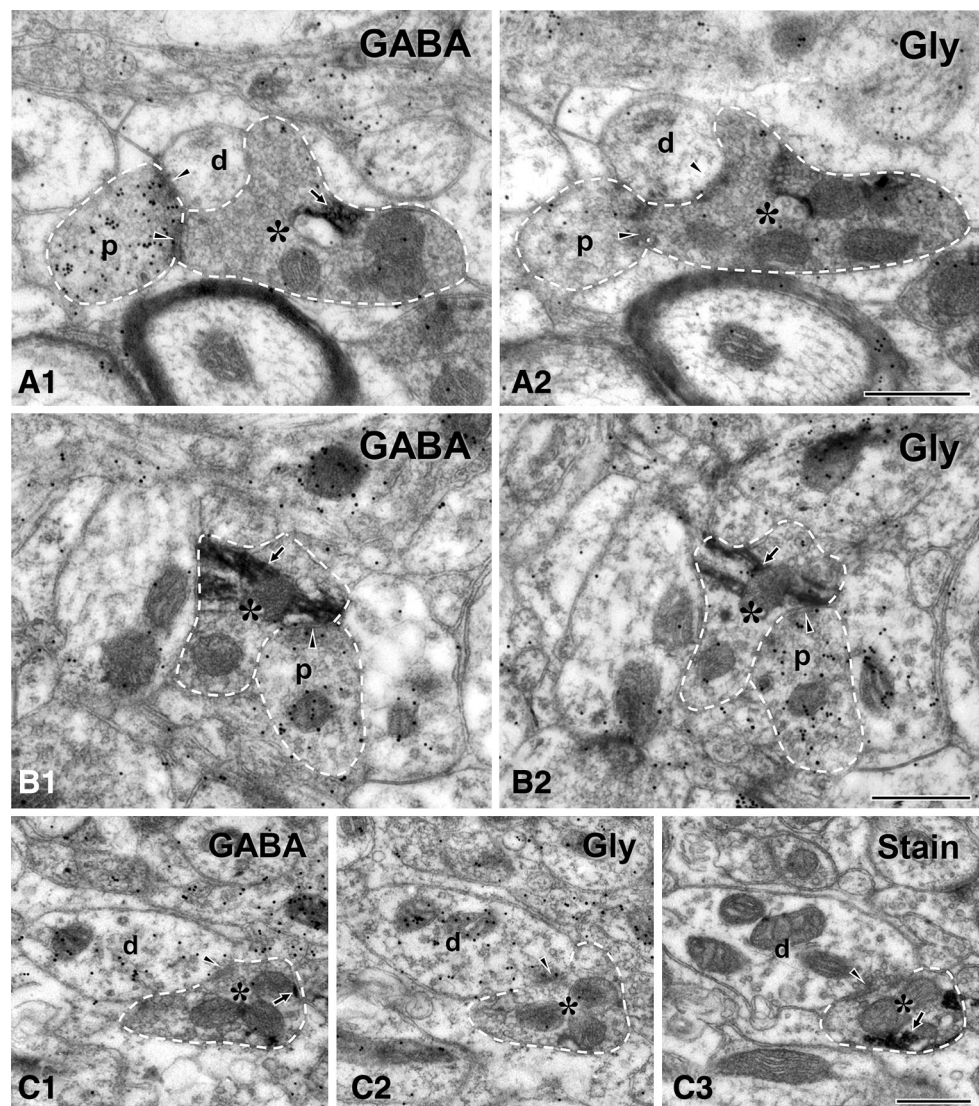
same type of fibers. The majority of the labeled boutons in the present study made synaptic contacts with one or two postsynaptic dendrites, suggesting that, at a single bouton level, gustatory signals are transmitted to one or two postsynaptic neurons, i.e., to a specific group of neurons with a small degree of synaptic divergence. This is similar to the connectivity of the terminals of Aβ LTM and peptidergic C afferents in the spinal dorsal horn (SDH) and the trigeminal sensory nuclei (TSN, Alvarez et al. 1993; Bae et al. 1994, 2005a). However, it differs from that of somatosensory Aδ afferents, which form complex synaptic arrangements with 3–13 postsynaptic dendrites (Alvarez et al. 1992); since each dendrite postsynaptic to a single axon terminal in these arrangements belongs to a different

Table 3 Comparison of ultrastructural parameters of HRP-labeled chorda tympani afferent boutons and their presynaptic endings (p-endings) in the central subdivision of the rostral nucleus of the solitary tract

Bouton types/ parameters	n	Volume (μm^3)	Mitochondrial volume (μm^3)[a]	Active zone area (μm^2)[a]	Vesicle density[b]
HRP-labeled boutons (range)	30	1.70 ± 1.04[c] (0.72–5.22)	0.29 ± 0.17[c] (0.03–0.76)	0.44 ± 0.36[c] (0.07–1.74)	88.26 ± 19.50 (59.34–127.74)
P-endings (range)	10	0.61 ± 0.32 (0.22–1.11)	0.11 ± 0.06 (0.01–0.19)	0.04 ± 0.02 (0.01–0.08)	94.60 ± 22.17 (54.74–122.80)

[a] Values for mitochondrial volume and active zone area are total values for each HRP-labeled bouton and p-ending

[b] Vesicle density indicated number of vesicles per unit area (μm^2)

[c] Indicates statistically significant differences between HRP-labeled boutons and p-endings (unpaired t test, $p < 0.05$)
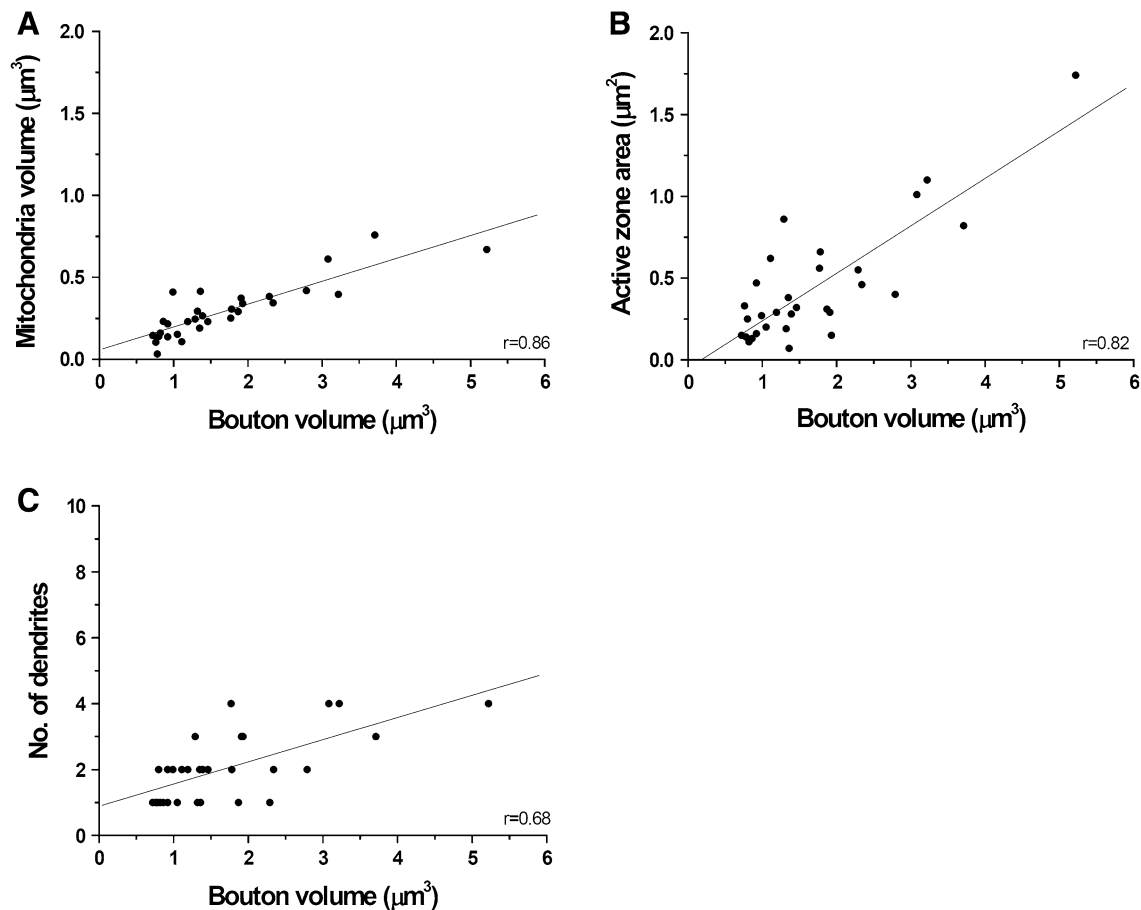
Fig. 6 Correlation between bouton volume of HRP-labeled chorda tympani afferents in the central subdivision of the rostral nucleus of the solitary tract and their mitochondrial volume (**a**), active zone area (**b**), and number of postsynaptic dendrites (**c**). r correlation coefficient

Table 4 Frequency of occurrence of p-profiles, which are presynaptic to the HRP-labeled chorda tympani bouton, according to the immunoreactivity for GABA and/or glycine in the central subdivision of the rostral nucleus of the solitary tract

No. of p-profiles examined	p-profile immunopositive to		
	GABA only	Both GABA and Glycine	Glycine only
45	73.3 % (33/45)	26.7 % (12/45)	0.0 % (0/45)

neuron (Yabuta et al. 1996; Yoshida et al. 2001), the somatosensory Aδ afferents are likely to drive multiple postsynaptic neurons with a high degree of synaptic divergence at a single bouton level. It was reported that most of the rNST neurons show synapses characterized by having single or few contacts with the CT afferent fiber input (Wang and Bradley 2010). At present, little is known on how many boutons do a single CT afferent may have and on how many rNST neurons do a single CT afferent
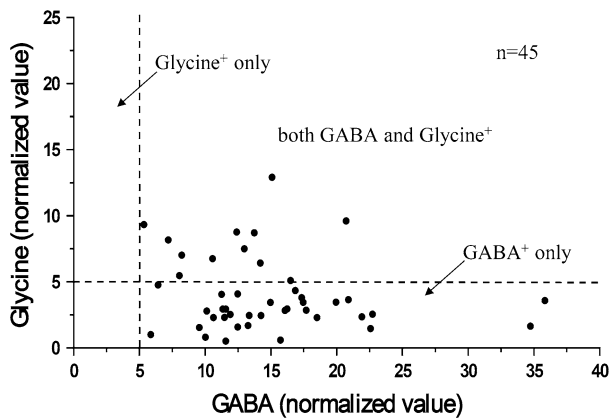
Fig. 7 Scatterplot showing normalized values of gold particle density (gold particle density in p-profile/background density) for GABA (abscissa) and glycine (ordinate) in individual p-profiles, which are presynaptic to labeled chorda tympani afferent boutons. Background density is an average from 10 to 15 axon terminals, which contain clear round vesicles and show asymmetrical synaptic contacts with dendrites or somata. A p-profile was considered immunopositive when the gold particle density over the vesicle-containing areas in the p-endings or the vesicle-rich area in the p-profile of presumed dendritic origin was five times higher than the background (*dashed lines*). P-endings immunopositive for GABA only also contain a small amount of glycine, but at levels below the arbitrary cutoff value for our analysis

contact. Further study on the synaptic divergence at a single CT afferent level is needed. Another difference is number of target regions: Thus, the rNST neurons project mainly to the parabrachial nucleus and the medullary reticular formation, and mediate taste perception and reflex motor activity, respectively (Streefland and Jansen 1999; Cho et al. 2002; Corson and Bradley 2013). Whereas the neurons in the superficial lamina of the medullary and

spinal dorsal horn, which receive input from somatosensory Aδ afferents, project to the thalamus and hypothalamus, among other brain regions (Keay et al. 1997; Li et al. 1997; Spike et al. 2003; Al-Khater et al. 2008). The smaller degree of synaptic divergence of the CT afferents at a single bouton level and the limited number of targets for projecting rNST neurons, compared to the somatosensory Aδ afferents and their postsynaptic neurons may reflect the relatively simpler aspect of taste sensation, compared to the more complex aspects of Aδ fiber-mediated somatic sensation, such as the perceptual and affective aspects of pain, the afferent limb of complex motor reflexes, etc.

Axoaxonic synapses are considered the morphological substrate for presynaptic modulation implicated in the sharpening of sensory transmission through lateral inhibition (Gray 1962). In our study, labeled boutons frequently received synapses from p-profiles, confirming previous observations (Whitehead 1986). The frequency of CT afferent boutons that receive synapses from p-profiles (25 %) and the number of the p-profiles per CT afferent bouton (∼1) was lower than that for the Aβ LTM afferent terminals (50–100 %, up to 9 p-endings; Bae et al. 1994, 2005a; Watson et al. 2002; Watson 2003, 2004), and for the Aδ HTM afferent terminals (20–60 %, up to 6 p-endings; Alvarez et al. 1992), but higher than that for the C afferent terminals, which do not participate in axoaxonic contacts (Alvarez et al. 1993). The degree of presynaptic modulation of the gustatory vs. somatosensory fibers may reflect the potential for spatial discrimination of sensory transmission mediated by each of the fiber types.

Previous electrophysiological studies showed that the responses of taste-sensitive NST neurons are suppressed by microinjection of GABA into the NST (Wang and Bradley
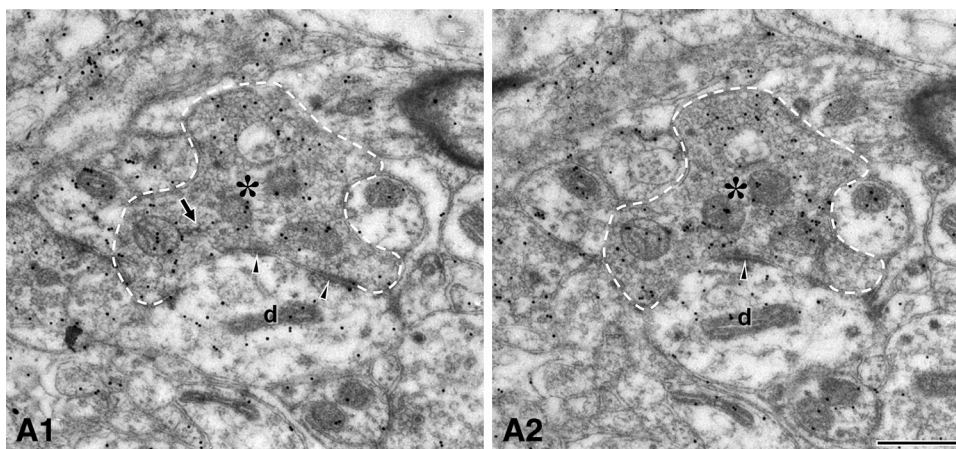

Fig. 8 Electron micrographs of serial thin sections showing an HRP-labeled chorda tympani afferent bouton (*asterisks*) in the central subdivision of the rostral nucleus of the solitary tract. The *arrow* indicates HRP reaction product, *arrowheads* indicate synapses; the labeled bouton is outlined with a *dashed line*. Adjacent ultrathin sections of the labeled bouton are immunostained for glutamate. The labeled bouton makes a synaptic contact with a dendrite (*d*) and is immunopositive for glutamate. *Scale bar* 500 nm

1993; Smith et al. 1994), suggesting that these neurons are under GABAergic inhibition. However, there has been little evidence of presynaptic modulation of the gustatory afferents by GABA. All p-profiles in the present study were GABA+ and considerable fractions were also glycine+ with the relative amount of GABA and glycine being different in each GABA/Gly+ p-profile. To the best of our knowledge, this provides the first morphological evidence that gustatory afferents receive GABAergic, as well as glycinergic, synaptic contacts on their terminals in the rNST, suggesting that gustatory signals conveyed via CT afferents receive GABA- and glycine-mediated presynaptic modulation. At present, little is known about the functional significance of the colocalization of GABA and glycine in a single p-profile. Co-release of GABA and glycine induces mixed miniature inhibitory postsynaptic currents (mixed mIPSC), which evoke stronger postsynaptic effects than the release of GABA or glycine alone (Keller et al. 2001; Russier et al. 2002). In addition, $GABA_A$ and glycine receptor show different decay time course; $GABA_A$ and glycine receptor-mediated mIPSC show slow and fast decay time, respectively (Jonas et al. 1998; Nabekura et al. 2004). Therefore, co-release of GABA and glycine at various ratios from each p-profile may also underlie the precise temporal regulation of the inhibitory input to the CT afferent bouton and its synaptic release. In the present study, gold particle density for glutamate was higher in labeled boutons than the average tissue density, reflecting metabolic glutamate, suggesting that labeled boutons contain neurotransmitter glutamate (Ottersen 1989a, b). This lends morphological support to electrophysiological studies showing that synaptic transmission between CT afferents and gustatory NST neurons is mediated by glutamate (for review, see Bradley et al. 1996; Li and Smith 1997; for review, see Smith et al. 1998).

The correlation between the volume of the CT afferent bouton and its ultrastructural features related to synaptic release, and the smaller volume of the presynaptic p-endings, are analogous to that of the somatosensory LTM and proprioceptive afferents (Pierce and Mendell 1993; Nakagawa et al. 1997; Paik et al. 2005; Moon et al. 2008). The smaller size of the p-ending, compared to that of the CT afferent bouton postsynaptic to it, suggests that the presynaptic inhibition exerted by the p-ending may require a small amount of inhibitory neurotransmitter to modulate the synaptic release from the CT afferent bouton by reducing the amplitude of action potentials arriving into the afferent bouton. The volume of the CT afferent bouton was also positively correlated with the number of its postsynaptic dendrites, suggesting that despite the larger overall amount of neurotransmitter released from large boutons, the amount of transmitter released onto a single postsynaptic dendrite may be similar.

References

Al-Khater KM, Kerr R, Todd AJ (2008) A quantitative study of spinothalamic neurons in laminae I, III, and IV in lumbar and cervical segments of the rat spinal cord. J Comp Neurol 511:1–18

Almeida TF, Roizenblatt S, Tufik S (2004) Afferent pain pathways: a neuroanatomical review. Brain Res 1000:40–56

Alvarez FJ, Kavookjian AM, Light AR (1992) Synaptic interactions between GABA-immunoreactive profiles and the terminals of functionally defined myelinated nociceptors in the monkey and cat spinal cord. J Neurosci 12:2901–2917

Alvarez FJ, Kavookjian AM, Light AR (1993) Ultrastructural morphology, synaptic relationships, and CGRP immunoreactivity of physiologically identified C-fiber terminals in the monkey spinal cord. J Comp Neurol 329:472–490

Bae YC, Nakagawa S, Yoshida A, Nagase Y, Takemura M, Shigenaga Y (1994) Morphology and synaptic connections of slowly adapting periodontal afferent terminals in the trigeminal subnuclei principalis and oralis of the cat. J Comp Neurol 348:121–132

Bae YC, Nakagawa S, Yasuda K, Yabuta NH, Yoshida A, Pil PK, Moritani M, Chen K, Nagase Y, Takemura M, Shigenaga Y (1996) Electron microscopic observation of synaptic connections of jaw-muscle spindle and periodontal afferent terminals in the trigeminal motor and supratrigeminal nuclei in the cat. J Comp Neurol 374:421–435

Bae YC, Ihn HJ, Park MJ, Ottersen OP, Moritani M, Yoshida A, Shigenaga Y (2000) Identification of signal substances made between primary afferents and their associated axon terminals in the rat trigeminal sensory nuclei. J Comp Neurol 418:299–309

Bae YC, Choi BJ, Lee MG, Lee HJ, Park KP, Zhang LF, Honma S, Fukami H, Yoshida A, Ottersen OP, Shigenaga Y (2002) Quantitative ultrastructural analysis of glycine- and gamma-aminobutyric acid-immunoreactive terminals on trigeminal alpha- and gamma-motoneuron somata in the rat. J Comp Neurol 442:308–319

Bae YC, Ahn HJ, Park KP, Kim HN, Paik SK, Bae JY, Lee HW, Kim KH, Yoshida A, Moritani M, Shigenaga Y (2005a) The synaptic microcircuitry associated with primary afferent terminals in the interpolaris and caudalis of trigeminal sensory nuclear complex. Brain Res 1060:118–125

Bae YC, Park KS, Bae JY, Paik SK, Ahn DK, Moritani M, Shigenaga Y, Yoshida A (2005b) GABA and glycine in synaptic microcircuits associated with physiologically characterized primary afferents of cat trigeminal principal nucleus. Exp Brain Res 162:449–457

Barret KE, Barman SM, Boitano S, Brooks H (2009) Excitable tissue: nerve. In: Barret KE, Barman SM, Boitano S, Brooks H (eds) Ganong's review of medical physiology, 23rd edn. McGraw-Hill Medical, New York, pp 79–92

Biedenbach MA, Chan KY (1971) Tongue mechanoreceptors: comparison of afferent fibers in the lingual nerve and chorda tympani. Brain Res 35:584–588

Bradley RM, King MS, Wang L, Shu X (1996) Neurotransmitter and neuromodulator activity in the gustatory zone of the nucleus tractus solitarius. Chem Senses 21:377–385

Cho YK, Li CS, Smith DV (2002) Gustatory projections from the nucleus of the solitary tract to the parabrachial nuclei in the hamster. Chem Senses 27:81–90

Corson JA, Bradley RM (2013) Physiological and anatomical properties of intramedullary projection neurons in rat rostral nucleus of the solitary tract. J Neurophysiol 110:1130–1143

Corson J, Aldridge A, Wilmoth K, Erisir A (2012) A survey of oral cavity afferents to the rat nucleus tractus solitarii. J Comp Neurol 520:495–527

Craig AD (2002) How do you feel? Interoception: the sense of the physiological condition of the body. Nat Rev Neurosci 3:655–666

Davis BJ (1993) GABA-like immunoreactivity in the gustatory zone of the nucleus of the solitary tract in the hamster: light and electron microscopic studies. Brain Res Bull 30:69–77

Davis BJ (1998) Synaptic relationships between the chorda tympani and tyrosine hydroxylase-immunoreactive dendritic processes in the gustatory zone of the nucleus of the solitary tract in the hamster. J Comp Neurol 392:78–91

Debanne D, Campanac E, Bialowas A, Carlier E, Alcaraz G (2011) Axon physiology. Physiol Rev 91:555–602

Farbman AI, Hellekant G (1978) Quantitative analyses of the fiber population in rat chorda tympani nerves and fungiform papillae. Am J Anat 153:509–521

Fyffe RE, Light AR (1984) The ultrastructure of group Ia afferent fiber synapses in the lumbosacral spinal cord of the cat. Brain Res 300:201–209

Grant G (2006) The 1932 and 1944 Nobel Prizes in physiology or medicine: rewards for ground-breaking studies in neurophysiology. J Hist Neurosci 15:341–357

Gray EG (1962) A morphological basis for pre-synaptic inhibition? Nature 193:82–83

Harper AA, Lawson SN (1985) Conduction velocity is related to morphological cell type in rat dorsal root ganglion neurones. J Physiol 359:31–46

Iriuchijima J, Zotterman Y (1961) Conduction rates of afferent fibres to the anterior tongue of the dog. Acta Physiol Scand 51:283–289

Jonas P, Bischofberger J, Sandkuhler J (1998) Corelease of two fast neurotransmitters at a central synapse. Science 281:419–424

Keay KA, Feil K, Gordon BD, Herbert H, Bandler R (1997) Spinal afferents to functionally distinct periaqueductal gray columns in the rat: an anterograde and retrograde tracing study. J Comp Neurol 385:207–229

Keller AF, Coull JA, Chery N, Poisbeau P, De Koninck Y (2001) Region-specific developmental specialization of GABA-glycine cosynapses in laminas I-II of the rat spinal dorsal horn. J Neurosci 21:7871–7880

King MS (2006) Anatomy of the rostral nucleus of the solitary tract. In: Bradley RM (ed) The role of the nucleus of the solitary tract in gustatory processing. CRC Press, Boca Raton, pp 17–38

Kishimoto H, Bae YC, Yoshida A, Moritani M, Takemura M, Nakagawa S, Nagase Y, Wada T, Sessle BJ, Shigenaga Y (1998) Central distribution of synaptic contacts of primary and secondary jaw muscle spindle afferents in the trigeminal motor nucleus of the cat. J Comp Neurol 391:50–63

Kitamura K, Kimura RS, Schuknecht HF (1982) The ultrastructure of the geniculate ganglion. Acta Otolaryngol 93:175–186

Lasiter PS, Kachele DL (1988) Organization of GABA and GABA-transaminase containing neurons in the gustatory zone of the nucleus of the solitary tract. Brain Res Bull 21:623–636

Lawson SN, Waddell PJ (1991) Soma neurofilament immunoreactivity is related to cell size and fibre conduction velocity in rat primary sensory neurons. J Physiol 435:41–63

Lawson SN, Crepps BA, Perl ER (1997) Relationship of substance P to afferent characteristics of dorsal root ganglion neurones in guinea-pig. J Physiol 505:177–191

Lawson SN, Crepps B, Perl ER (2002) Calcitonin gene-related peptide immunoreactivity and afferent receptive properties of dorsal root ganglion neurones in guinea-pigs. J Physiol 540:989–1002

Leonard NL, Renehan WE, Schweitzer L (1999) Structure and function of gustatory neurons in the nucleus of the solitary tract. IV. The morphology and synaptology of GABA-immunoreactive terminals. Neuroscience 92:151–162

Li CS, Smith DV (1997) Glutamate receptor antagonists block gustatory afferent input to the nucleus of the solitary tract. J Neurophysiol 77:1514–1525

Li JL, Kaneko T, Shigemoto R, Mizuno N (1997) Distribution of trigeminohypothalamic and spinohypothalamic tract neurons displaying substance P receptor-like immunoreactivity in the rat. J Comp Neurol 378:508–521

Matsuo R, Inoue T, Masuda Y, Nakamura O, Yamauchi Y, Morimoto T (1995) Neural activity of chorda tympani mechanosensitive fibers during licking behavior in rats. Brain Res 689:289–298

May OL, Erisir A, Hill DL (2007) Ultrastructure of primary afferent terminals and synapses in the rat nucleus of the solitary tract: comparison among the greater superficial petrosal, chorda tympani, and glossopharyngeal nerves. J Comp Neurol 502: 1066–1078

Moon YS, Paik SK, Seo JH, Yi HW, Cho YS, Moritani M, Yoshida A, Ahn DK, Kim YS, Bae YC (2008) GABA- and glycine-like immunoreactivity in axonal endings presynaptic to the vibrissa afferents in the cat trigeminal interpolar nucleus. Neuroscience 152:138–145

Nabekura J, Katsurabayashi S, Kakazu Y, Shibata S, Matsubara A, Jinno S, Mizoguchi Y, Sasaki A, Ishibashi H (2004) Developmental switch from GABA to glycine release in single central synaptic terminals. Nat Neurosci 7:17–23

Nakagawa S, Kurata S, Yoshida A, Nagase Y, Moritani M, Takemura M, Bae YC, Shigenaga Y (1997) Ultrastructural observations of synaptic connections of vibrissa afferent terminals in cat principal sensory nucleus and morphometry of related synaptic elements. J Comp Neurol 389:12–33

Ogawa H, Sato M, Yamashita S (1968) Multiple sensitivity of chorda tympani fibres of the rat and hamster to gustatory and thermal stimuli. J Physiol 199:223–240

Ogawa H, Imoto T, Hayama T (1984) Responsiveness of solitario-parabrachial relay neurons to taste and mechanical stimulation applied to the oral cavity in rats. Exp Brain Res 54:349–358

Ottersen OP (1987) Postembedding light- and electron microscopic immunocytochemistry of amino acids: description of a new model system allowing identical conditions for specificity testing and tissue processing. Exp Brain Res 69:167–174

Ottersen OP (1989a) Postembedding immunogold labelling of fixed glutamate: an electron microscopic analysis of the relationship between gold particle density and antigen concentration. J Chem Neuroanat 2:57–66

Ottersen OP (1989b) Quantitative electron microscopic immunocytochemistry of neuroactive amino acids. Anat Embryol (Berl) 180:1–15

Ottersen OP, Storm-Mathisen J, Madsen S, Skumlien S, Strømhaug J (1986) Evaluation of the immunocytochemical method for amino acids. Med Biol 64:147–158

Paik SK, Oh SJ, Son YJ, Ma SK, Ahn CH, Kim SK, Chang Z, Moritani M, Yoshida A, Bae YC (2005) Neural mechanisms controlling jaw-jerk reflex in the cat. NeuroReport 16:1565–1568

Paik SK, Bae JY, Park SE, Moritani M, Yoshida A, Yeo EJ, Choi KS, Ahn DK, Moon C, Shigenaga Y, Bae YC (2007) Developmental changes in distribution of gamma-aminobutyric acid- and glycine-immunoreactive boutons on rat trigeminal motoneurons. I. Jaw-closing motoneurons. J Comp Neurol 503:779–789

Paik SK, Park SK, Jin JK, Bae JY, Choi SJ, Yoshida A, Ahn DK, Bae YC (2011) Ultrastructural analysis of glutamate-immunopositive synapses onto the rat jaw-closing motoneurons during postnatal development. J Neurosci Res 89:153–161

Paik SK, Kwak MK, Bae JY, Yi HW, Yoshida A, Ahn DK, Bae YC (2012) γ-aminobutyric acid-, glycine-, and glutamate-immunopositive boutons on mesencephalic trigeminal neurons that innervate jaw-closing muscle spindles in the rat: ultrastructure and development. J Comp Neurol 520:3414–3427

Pierce JP, Mendell LM (1993) Quantitative ultrastructure of Ia boutons in the ventral horn: scaling and positional relationships. J Neurosci 13:4748–4763

Robinson PP (1988) The characteristics and regional distribution of afferent fibres in the chorda tympani of the cat. J Physiol 406:345–357

Russier M, Kopysova IL, Ankri N, Ferrand N, Debanne D (2002) GABA and glycine co-release optimizes functional inhibition in rat brainstem motoneurons in vitro. J Physiol 541:123–137

Shigenaga Y, Moritani M, Oh SJ, Park KP, Paik SK, Bae JY, Kim HN, Ma SK, Park CW, Yoshida A, Ottersen OP, Bae YC (2005) The distribution of inhibitory and excitatory synapses on single, reconstructed jaw-opening motoneurons in the cat. Neuroscience 133:507–518

Smith DV, Liu H, Vogt MB (1994) Neural coding of aversive and appetitive gustatory stimuli: interactions in the hamster brain stem. Physiol Behav 56:1189–1196

Smith DV, Li CS, Davis BJ (1998) Excitatory and inhibitory modulation of taste responses in the hamster brainstem. Ann N Y Acad Sci 855:450–456

Spassova I (1983) Fine structure of the neurons of the geniculate ganglion of the cat. J Hirnforsch 24:123–133

Spike RC, Puskár Z, Andrew D, Todd AJ (2003) A quantitative and morphological study of projection neurons in lamina I of the rat lumbar spinal cord. Eur J Neurosci 18:2433–2448

Storm-Mathisen J, Leknes AK, Bore AT, Vaaland JL, Edminson P, Haug FM, Ottersen OP (1983) First visualization of glutamate and GABA in neurones by immunocytochemistry. Nature 301:517–520

Streefland C, Jansen K (1999) Intramedullary projections of the rostral nucleus of the solitary tract in the rat: gustatory influences on autonomic output. Chem Senses 24:655–664

Takumi Y, Ramírez-León V, Laake P, Rinvik E, Ottersen OP (1999) Different modes of expression of AMPA and NMDA receptors in hippocampal synapses. Nat Neurosci 2:618–624

Travers SP, Norgren R (1995) Organization of orosensory responses in the nucleus of the solitary tract of rat. J Neurophysiol 73:2144–2162

Walmsley B, Wieniawa-Narkiewicz E, Nicol MJ (1987) Ultrastructural evidence related to presynaptic inhibition of primary muscle afferents in Clarke's column of the cat. J Neurosci 7:236–243

Walmsley B, Graham B, Nicol MJ (1995) Serial E-M and simulation study of presynaptic inhibition along a group Ia collateral in the spinal cord. J Neurophysiol 74:616–623

Wang L, Bradley RM (1993) Influence of GABA on neurons of the gustatory zone of the rat nucleus of the solitary tract. Brain Res 616:144–153

Wang L, Bradley RM (1995) In vitro study of afferent synaptic transmission in the rostral gustatory zone of the rat nucleus of the solitary tract. Brain Res 702:188–198

Wang M, Bradley RM (2010) Synaptic characteristics of rostral nucleus of the solitary tract neurons with input from the chorda tympani and glossopharyngeal nerves. Brain Res 1328:71–78

Wang S, Corson J, Hill D, Erisir A (2012) Postnatal development of chorda tympani axons in the rat nucleus of the solitary tract. J Comp Neurol 520:3217–3235

Watson AH (2003) GABA- and glycine-like immunoreactivity in axons and dendrites contacting the central terminals of rapidly adapting glabrous skin afferents in rat spinal cord. J Comp Neurol 464:497–510

Watson AH (2004) Synaptic interactions between the terminals of slow-adapting type II mechanoreceptor afferents and neurones expressing gamma-aminobutyric acid- and glycine-like immunoreactivity in the rat spinal cord. J Comp Neurol 471:168–179

Watson AH, Hughes DI, Bazzaz AA (2002) Synaptic relationships between hair follicle afferents and neurones expressing GABA and glycine-like immunoreactivity in the spinal cord of the rat. J Comp Neurol 452:367–380

Weinberg RJ, van Eyck SL (1991) A tetramethylbenzidine/tungstate reaction for horseradish peroxidase histochemistry. J Histochem Cytochem 39:1143–1148

Wetherton BM, Leonard NL, Renehan WE, Schweitzer L (1998) Structure and function of gustatory neurons in the nucleus of the solitary tract. III. Classification of terminals using cluster analysis. Biotech Histochem 73:164–173

Whitehead MC (1986) Anatomy of the gustatory system in the hamster: synaptology of facial afferent terminals in the solitary nucleus. J Comp Neurol 224:72–85

Whitehead MC (1993) Distribution of synapses on identified cell types in a gustatory subdivision of the nucleus of the solitary tract. J Comp Neurol 332:326–340

Yabuta NH, Yasuda K, Nagase Y, Yoshida A, Fukunishi Y, Shigenaga Y (1996) Light microscopic observations of the contacts made between two spindle afferent types and alpha-motoneurons in the cat trigeminal motor nucleus. J Comp Neurol 374:436–450

Yoshida A, Fukami H, Nagase Y, Appenteng K, Honma S, Zhang LF, Bae YC, Shigenaga Y (2001) Quantitative analysis of synaptic contacts made between functionally identified oralis neurons and trigeminal motoneurons in cats. J Neurosci 21:6298–6307

Zhang LF, Moritani M, Honma S, Yoshida A, Shigenaga Y (2001) Quantitative ultrastructure of slowly adapting lingual afferent terminals in the principal and oral nuclei in the cat. Synapse 41:96–111

Zhang J, Pendlebury WW, Luo P (2003) Synaptic organization of monosynaptic connections from mesencephalic trigeminal nucleus neurons to hypoglossal motoneurons in the rat. Synapse 49:157–169